Title: Individual reflectance of solar radiation as a thermoregulatory adaptation to microclimate: A test in dimorphic male bees (*Centris pallida)*

Short Title: Microclimate Impacts UV-NIR Reflectance in Dimorphic Bees

Authors: Barrett M[1*], O'Donnell S[1,2]

Affiliations:

[1]Department of Biology, Drexel University, Philadelphia, PA

[2]Department of Biodiversity, Earth, and Environmental Sciences, Drexel University, Philadelphia PA

[*]corresponding author: meghan.barrett21@gmail.com; 3245 Chestnut St, Philadelphia, PA 19104

Keywords: shortwave radiation, external reflectance, solitary bees, alternative reproductive tactics

Declarations of Interest: none.

Abstract

Incoming solar radiation (wavelengths 290 – 2500 nm) significantly impacts an organism's thermal balance via radiative heat gain. Species adapted to different environments can differ in solar reflectance profiles. We hypothesized that conspecific individuals using thermally distinct microhabitats to engage in fitness-relevant behaviors would show intraspecific differences in reflectance: we predicted individuals that use hot microclimates (where radiative heat gain represents a greater thermoregulatory challenge) would be more reflective across the entire solar spectrum than those using cooler microclimates. Differences in near-infrared (NIR) reflectance (700 - 2500 nm) are strongly indicative of thermoregulatory adaptation as, unlike differences in visible reflectance (400 - 700 nm), they are not perceived by ecological or social partners. We tested these predictions in male *Centris pallida* (Hymenoptera: Apidae) bees from the Sonoran Desert. Male *C. pallida* use alternative reproductive tactics that are associated with distinct microclimates: Large-morph males, with paler visible coloration, behave in an extremely hot microclimate close to the ground, while small-morph males, with a dark brown dorsal coloration, frequently use cooler microclimates above the ground near vegetation. We found that large-morph males had increased reflectance of solar radiation (UV through NIR) resulting in lower solar absorption coefficients. This thermoregulatory adaptation was specific to the dorsal surface, and produced by differences in hair, not cuticle, characteristics. Our results showed that intraspecific variation in behavior, particular in relation to microclimate use, can generate unique thermal adaptations that changes the reflectance of shortwave radiation among individuals within the same population.

Introduction

Solar (shortwave) radiation plays a large role in an organism's thermoregulation via radiative heat gain, driving adaptive patterns of body coloration and reflectance (Stuart-Fox et al. 2017, Munro et al. 2019). Organisms may absorb solar energy to heat up, or transmit/reflect solar energy to avoid additional heat gain (Amore et al. 2017, Gomez et al. 2021). Environmental conditions are particularly important for ectotherms, which rely heavily on managing the influence of abiotic factors like shortwave radiation to maintain non-lethal body temperatures (Huey and Kingsolver 1989). Differences in reflectance across the entire solar ultraviolet (UV) to near infrared (NIR) spectrum can thus have significant thermoregulatory consequences (Krishna et al. 2020; Wang et al. 2021); for example, the reflective hairs of Saharan silver ants reduce their body temperatures by as much as 7-10 °C (Shi et al. 2015). The thermal effects of variation in solar radiation affect population and species variation in color and reflectance across landscapes (Spicer and Gaston 1999; Willig et al. 2003; Munro et al. 2019; Gomez et al. 2021, Kang et al. 2021, Medina et al. 2018).

Differences in ectotherms' visible coloration (henceforth, VIS reflectance, wavelengths 400 - 700 nm) can serve as a morphological mechanism for thermal adaptation (e.g. Thermal Melanism Hypothesis or Bogert's Rule; Bogert, 1949; Schultz and Hadley 1987; Clusella-Trullas et al. 2007, Hegna et al. 2013). External coloration impacts operative temperatures both across and within lizard species (Cole 1943; Smith et al. 2016). However, climate is a poor predictor of visible color in butterflies, and ant assemblages demonstrate conflicting macrophysiological coloration patterns (Bishop et al. 2016; Schofield et al. 2016; Munro et al. 2019). These conflicting patterns may result from the fact that VIS reflectance is under selection by factors not related to thermoregulation, including social/sexual signaling and anti-predator adaptations,

which may conflict with thermal selective effects (e.g., Hegna et al. 2013, Stuart-Fox et al. 2017). By contrast, differences in external reflectance of NIR (701 – 2500 nm) radiation are not confounded by ecological and social partners, and are thus generally only under selection for thermoregulatory reasons (Stuart-Fox et al. 2017). NIR reflectance has larger impacts on heating rates than VIS reflectance (Wang et al. 2021), and is more consistently associated with climate variation (Shi et al. 2015; Munro et al. 2019, Kang et al. 2021, Gomez et al. 2021).

Research on adaptive coloration and reflectance has focused on population or species differences (Baudier et al. 2018, Spacht et al. 2021). However, there can be significant differences in body temperature associated with radiative heat gain in different microhabitats (e.g., sunny vs. shaded sites ; Kaspari et al. 2014). Within populations, individuals may vary consistently in which microhabitats they use based on their behaviors, with significant thermoregulatory consequences (Baudier et al. 2015, Kaspari et al. 2014, Cerdá et al. 1998, Van Dyck & Matthysen 1998, Cuesta & Lobo 2019). These individual differences are overlooked by population- and species-level studies, which treat conspecific individuals as ecologically equivalent despite the fact that individual variation can impact ecological and evolutionary dynamics and serves as a major target of natural selection (Bolnick et al. 2003). Studies that measure within-population differences can yield new insights into the selective pressures that act on individuals to generate evolutionary adaptations to fine-scale thermal variation.

Centris pallida bees live in the Sonoran Desert and experience extremely high temperatures during their mating aggregations (Chappell et al. 1984). Males are dimorphic in behavior and morphology: large-morph males patrol near the ground, fully exposed to the sun, and attempt to locate females in underground nests using scent. Large-morph males then dig out and fight over females, which can last 19 minutes or more (Alcock et al. 1977). Small-morph

83 males occasionally participate in this strategy, but more typically hover 1 m or more above the
84 ground near vegetation and chase after flying females they locate visually (Alcock 1976, Alcock
85 *et al.* 1976, Alcock *et al.* 1977, Alcock 2013). Air temperature in the typical large male
86 microclimate is nearly 10 °C hotter than the typical small male microclimate by the time mating
87 behaviors cease, around 1000 - 1100 hr (Barrett et al. 2022).

88 Large-morph males are paler in visible coloration than small-morph males and females
89 (Figure 1); however, increased VIS reflectance may be driven in part by the need to camouflage
90 themselves against the desert soil to reduce predation events by birds and lizards (Alcock 1995).
91 If the increased reflectance of large-morph males extends into the NIR, it likely represents a
92 thermoregulatory adaptation to reduce their radiative heat gain in the hotter microclimate. The
93 darker coloration of small-morph males may also be thermally adaptive, allowing them to
94 maximize performance during cooler early-morning periods when males are observed to bask on
95 bushes prior to foraging/mating around 0700 (Barrett, pers. comm.). Radiative heat gain is
96 critical at low air temperatures (particularly for flying insects that lose heat via convective
97 cooling, Van Dyck & Matthysen 1998), and plays a large role in allowing ectotherms to reach
98 active temperatures at cool air temperatures (Kingsolver 1983b). Females, which emerge even
99 earlier in the cool mornings to forage than small-morph males (Barrett, pers. comm), may also be
100 darker in coloration in order to increase solar radiative heat gain and maximize foraging
101 performance.

102 We hypothesized that microclimate usage drives morph-specific differences in UV-NIR
103 reflectance. We predicted that large-morph males would have increased reflectance of solar
104 radiation compared to small-morph males, as a thermoregulatory adaptation to reduce or increase
105 shortwave radiative heat gain in their hotter or cooler microclimates, respectively. Because

106 microhabitat differences are strongest in incident radiation from above, we predicted morph
107 reflectance differences on the dorsal, but not ventral, body surfaces (see Shi et al. 2015). To
108 better understand mechanisms of morph-specific reflectance we tested whether differences in
109 reflectance were related to hair (branched setae) or cuticle characteristics; we measured solar
110 reflectance of the dorsal surface of the thorax with, and without, hairs present. We predicted that
111 hair density would correlate with increased reflectance across body regions, or morph/sex, and
112 calculated hair density on the thorax and abdomen across morphs and females. Finally, we
113 predicted that females would have similar reflectance profiles to small-morph males on the
114 dorsal surface, and would not differ from males in ventral surface reflectance.

115 **Materials and Methods**

116 ***Specimen Collection***

117 We classified males as the 'large' male morph if we found them patrolling, digging, or
118 fighting and they had the grey/white coloration (Figure 1, Supplementary Figure 1) and leg
119 morphology distinctive to the large, behaviorally-inflexible morph (Alcock 1976, Alcock *et al.*
120 1977, Snelling 1984). We classified them as 'small' male morphs if we collected them hovering
121 near vegetation (large-morph males never engage in hovering behavior; Alcock *et al.* 1977). We
122 collected *C. pallida* males and females (n = 10/morph or sex) in late April and early May of 2018
123 in the floodplain of the Salt River, in Arizona (N33.552, W111.566), or in late April and early
124 May of 2019, approximately ~10 km away from the first location (N33.464, W111.632). We
125 transported bees in a cooler on ice to a lab where we weighed them on an analytical balance
126 (Metler Toledo AB54-S) to the nearest 0.1 mg.

127

Figure 1. Visible coloration and size dimorphism in *C. pallida*. Large-morph *C. pallida* male (left) has a larger body size and a pale-grey coloration across the head, thorax, and abdomen compared to the small-morph *C. pallida* male (middle), which has a brown head and thorax and dark grey abdomen, most similar to the female of generally intermediate size (right). Close-up photos of thorax and abdomen coloration in Supplementary Figure 1.

Morphological Measurements

We used digital calipers (Husky, 6 inch - 3 mode model) to measure the body parts of the male and female bees used for reflectance spectrophotometry. We assumed the thorax and head to be a single cylinder for surface area calculations, with a diameter was equal to the widest point of the thorax and height equal to the length of the bee from the top of the head to the back of the thorax. We assumed the abdomen was a cylinder with a diameter equal to the width of the second tergite, and height equal to the length of the abdomen. For surface area calculations, we subtracted one flat, circular side (e.g., base) of both the thorax-head, and abdomen, cylinders, in order to account for the surface where the abdomen and thorax meet.

Reflectance Spectrophotometry

We stored males of each morph and females dry, and away from light, following field collection. We captured total diffuse and spectral ultraviolet to near-infrared (290 - 2500 nm) percent reflectance (R) of the external surface using a Cary 5000 spectrophotometer equipped with an Agilent integrating sphere, deuterium arc (<350 nm) and tungsten-halogen (>350 nm) lamps, and R928 photomultiplier and PbS IR detectors. We limited measurements to a consistent diameter for all specimen using a custom aluminum aperture (2.18 mm diameter, 0.66 mm thickness), which we also used during the zero and baseline (Labsphere certified reflectance

standard, Spectralon) measurements. We set integration time to 0.2 seconds, with data intervals of 1 nm. Baseline measurements varied across set up days, possibly due to minor contamination on the Spectralon surface, so we used the following formula to standardize measurements ($R_{standardized,n}$) across different set-ups:

$$R_{standardized,n} = R_n \frac{(B_{Day1-100\%} - B_{Day1-0\%})}{(B_{n-100\%} - B_{n-0\%})}$$

Where R_n is the measured percent reflectance on Day n, $B_{100\%}$ is the Spectralon baseline (on Day 1 through Day n) and $B_{0\%}$ is the zero baseline (on Day 1 through Day n).

We measured R on the dorsal surface of the thorax (unshaved, and shaved of all hairs using a razor blade and the tips of #5 forceps), the dorsal surface of the abdomen on the first two terga, and the ventral surface of the abdomen on terga 2-3, for each specimen. We mounted specimen so that the thorax or abdomen was flat against the aperture, with measurements normal to the surface. Measurement error occurred between 799 and 800 nm due to the detector switching from the R928 to PbS IR (an artefact of sample orientation changing in relation to the new detector). To account for this, we averaged the difference in R between 799 and 800 and then added this value to all measurements ≤ 799 and subtracted it from all values ≥ 800. As *C. pallida* can lose hair over their lifetime, we only used individuals collected when the aggregation had just started, with low wing wear and no visible hair thinning on the thorax.

We assumed transmission through the bee was 0, and calculated average absorption (a_n) for a morph or sex at a wavelength 'n', using the following equation:

$$\overline{a_n} = 1 - \overline{R_n}$$

where $\overline{R}_n$ was the average fraction of reflectance of all ten specimen at wavelength n.

Solar Radiation Calculations

173 Thermal flux due to solar radiation can be defined by summing direct beam (b), diffuse
174 sky (d), and reflected (from substrates; r) radiation:

175 $$Q_{solar} = \overline{a_b} A_b I_b + \overline{a_d} A_d I_d + \overline{a_r} A_r I_r$$

176 where $\overline{a}$ is the absorption coefficient of the bee (the fraction of beam, diffuse, or reflected
177 radiation absorbed by the bee); A_b, A_d, and A_r are the surface area of the bee exposed to beam,
178 diffuse, or reflected radiation; and I_b, I_d, and I_r is the total irradiance of the beam, diffuse, or
179 reflected source. Here, we assumed $A_b = 0.25\ A_s$ (total surface area), and A_d and $A_r = 0.5\ A_s$. For
180 A_b and A_d, we used the total thorax and abdomen surface areas separately for A_s, in order to take
181 advantage of the two distinct absorption coefficients we calculated for each region dorsally; for
182 A_r, we combined the two regions into a total surface area. Because only male morphs
183 consistently differ in surface area, we did not perform thermal flux calculations for females; we
184 did, however, calculate their absorption coefficients as described below.

185 We obtained the direct normal irradiance spectra in order to calculate $\overline{a_b}$ and $\overline{a_r}$ from the
186 National Renewable Energy Laboratory (ASTM G173-03 Reference Air Mass 1.5 Spectra
187 Derived from SMARTS v. 2.9.2; Gueymard et al. 2002). We calculated the direct beam
188 absorption coefficient (a_b) for each individual on the dorsal surface of the abdomen and the
189 thorax, as well as the shaved cuticle, between 290 and 2500 nm (λ_{min} and λ_{max}) as:

190 $$\overline{a_b} = \frac{\sum_{\lambda_{min}}^{\lambda_{max}} a_n I_n}{I_b}$$

191 Where I_n is the intensity of solar radiation at wavelength n and I_b is the total direct beam
192 irradiance between the min and max wavelengths.

193 We obtained the spectrum of radiation reflected from a light soil substrate ($RS^{substrate}$), at
194 each wavelength (n), from the USGS Spectral Library (sample ID: splib07a record = 13249;

Kokaly et al. 2017), in order to calculate the intensity of reflected radiation, I_r, based on the intensity of direct beam solar radiation (I_b) at each wavelength (n).

$$I_r = \sum_{\lambda_{min}}^{\lambda_{max}} I_n^{beam} \times RS_n^{substrate}$$

We then calculated the average absorption coefficient ($\overline{a_r}$) of reflected radiation, using each bee's ventral abdominal absorption (a_{rn}) coefficient at each wavelength (n):

$$\overline{a_r} = \frac{\sum_{\lambda_{min}}^{\lambda_{max}} a_{rn}(I_n^{beam} \times RS_n^{substrate})}{I_r}$$

We also calculated a second measure of I_r using an albedo measurement of light sand from the Sonoran Desert ($I_r = 0.245 I_b$; Marion et al. 2020), to compare with the light soil substrate spectrum obtained from the USGS spectral library. Unlike the USGS sample, this summed-reflectance value could not account for wavelength specific effects – but this value had the advantage of being from the location of interest.

We assumed $\overline{a_d}$ to be equal to $\overline{a_b}$ (as in Stupski and Schilder 2021). We assumed I_d was a 100 W/m^2 (Peterson and Dirmhirn 1981). We estimated direct beam radiation on April 20th, 2018 at 1000 hr using the following formula:

$$I_b = a_{cd}^{\left(\frac{1}{\sin\left(\emptyset * \left(\frac{\pi}{180}\right)\right)}\right)} * S_{po}$$

With the following assumptions: S_{po} =1361 W/m^2, a_{cd} =0.83 (clear day), and atmospheric pressure at the study site = standard air pressure (101.3 x 10^3 kPa). Altitude angle (ø) was calculated using the following equations, using the Julian date (J = 110), Latitude (32.2°, 0.562 rad [λ]), time (t = 1000), and solar noon time (t_0 = 1200):

$$hour\ angle: \theta = \frac{2\pi}{24}(t - t_0)$$

$$solar\ declination: \delta = 0.4102\ \cos(\frac{2\pi(J-172)}{365})$$

$$solar\ zenith\ angle\ (\zeta)\ \cos\zeta\ = (\sin\lambda\sin\delta) + (\cos\lambda\cos\delta\cos\theta)$$

$$altitude\ angle: \emptyset = 90 - (\zeta * \frac{180}{\pi})$$

Finally, We divided Q_{solar} by body mass (g) to determine solar radiative heat flux per unit of body mass.

Scanning Electron Microscopy

We shaved small patches of the second tergite of the abdomens of the specimen used for reflectance spectrophotometry (thoraxes were already shaved). We then mounted thoraxes and abdomens on metal stubs with electrically conductive tape and silver paint, before sputter-coating samples (Pt/Pd target, 80/20; Cressington 208 Hr Sputter Coater) for 40 s at 40 mA (approximately 8-10 nm deposition). We took three photos of the cuticular surface in three different places on the abdomen/thorax at 100X or 200X magnification using a Zeiss Supra 50VP (EHT set to 5 kV, high vacuum mode, SE2 detector). We used ImageJ to count the number of pores found at the base of the hairs within a standardized, circular region of 0.1 mm^2 area (centered on a pore) on each of the three photos for each individual, and averaged these three numbers to obtain hair density in terms of the number of hairs/mm^2. On the abdomen, both unbranched and branched setae can be found, however the pores that at the base of these two setae types are quite distinct (Figure 2); we counted only the pore type that led to the branched setae, which was more common.

Figure 2. Difference between pores of branched (hairs) and unbranched setae on the abdomen. A) Female abdominal cuticle, dorsal surface, with black arrowheads pointing to the locations of

unbranched setae pores (200X). This photo is representative of those used for quantification of hair density (taken on Terga 2). B) Terga 5 & 6 of a female *C. pallida* showing many unbranched setae (white arrowhead) against a background of generally shorter branched setae (black arrowhead; 50X). Unbranched setae appeared longer and more common on terminal terga. C) Female abdominal cuticle, showing difference in pores with branched (black arrowhead) and unbranched (white arrowhead) setae still attached on Terga 2 (1000X). D) Close-up of (A), showing difference in branched (black arrowhead) and unbranched (white arrowhead) setae pores (1000X).

Analyses

We used GraphPad Prism 9.1.2 (GraphPad Prism for Windows 2021) to analyze reflectance spectrophotometry, morphology, and hair density data. We used one-way ANOVAs with Tukey's MCT to compare body mass, and thorax and head or abdominal surface area across large/small males and females. We used a one-way ANOVA followed by Tukey's MCT for normally distributed data, or Kruskal-Wallis test with Dunn's MCT for data that were not normally distributed, to assess variation in hair density on the abdomen and thorax. We calculated mean percent reflectance in the UV (290-399), VIS (400-700) and NIR (split into "close NIR" [cNIR, 701 – 1400] and "far NIR" [fNIR, 1401 – 2500]) for each individual, and used a two-way RM ANOVA (with a Geisser-Greenhouse correction due to lack of sphericity in wavelength) to assess the impact of morph (e.g. large-morph male, small-morph male, and female), wavelength region (UV, VIS, close NIR, and far NIR), and individual differences in mean reflectance. When we found significant p-values for 'morph', we used a Tukey's MCT to assess variation across categorical morph assignments within each wavelength region (and

adjusted p-values for multiple comparisons). To test for differences in mean reflectance in the UV, VIS, cNIR, and fNIR between the shaved and unshaved dorsal thorax surface, or the dorsal and ventral side of the abdomen, of large and small males, we used two-way RM ANOVAs with Geisser-Greenhouse corrections. When we found significant p-values for the effect of 'shaving' (thorax) or 'side' (abdomen), we used a Bonferroni's MCT to assess variation associated with that variable within each wavelength region (and adjusted p-values for multiple comparisons). We used one-way ANOVAs followed by Bonferroni's MCTs were used to assess differences in absorption coefficients between morphs and females.

Results

Morphology & Hair Density

Large and small morph males, and females differed in their wet body masses (Table 1; One-way ANOVA: $F = 42.80$, $df = 32$, $p < 0.0001$). Large-morph males had increased abdomen, and thorax + head, surface areas compared to both small-morph males and females (Table 1; thorax and head SA: $F = 53.70$, $df = 32$, $p < 0.0001$; abdomen SA: $F = 40.25$, $df = 32$, $p < 0.0001$); small-morph males had slightly reduced abdomen ($q = 3.67$, $p = 0.0369$), but not thorax + head, surface areas ($q = 3.21$, $p = 0.09$), compared to females.

Table 1. Differences between male morphs and females in their surface area and body mass (n = 10; One-way ANOVAs with Tukey's MCT). Different letters indicate statistically significant differences ($p < 0.05$), among morphs/sexes in that variable.

Variable	Morph/Sex	Mean ± SD	Range
Abdomen – Surface Area (mm²)			
	LM[a]	453.0 ± 34.9	399.9 – 510.3
	SM[b]	327.6 ± 27.0	292.9 – 368.6
	F[c]	368.1 ± 44.6	316.9 – 449.5
Thorax and Head – Surface Area (mm²)			
	LM[a]	489.1 ± 45.3	421.8 – 584.1
	SM[b]	332.8 ± 29.4	271.1 – 360.7
	F[b]	370.9 ± 40.4	302.5 – 431.6
Wet Body Mass (g)			
	LM[a]	0.27 ± 0.05	0.19 – 0.34
	SM[c]	0.14 ± 0.02	0.11 – 0.19
	F[b]	0.19 ± 0.03	0.14 – 0.23

Hair density also differed across the abdomen and thorax dorsal surfaces based on sex/morph (Table 2, Figure 3; One-way ANOVA, abdomen: $F = 59.14$, $df = 27$, $p < 0.0001$; Kruskal-Wallis, thorax: K-W = 11.44, $p = 0.0033$). Large-morph males had more densely hairy abdomens and thoraxes than small-morph males (thorax: $Z = 3.23$, $p = 0.0037$; abdomen: $q = 3.84$, $df = 27$, $p = 0.0299$). Females did not differ from small-morph males in thorax hair density ($Z = 0.74$, $p > 0.99$), but had increased abdomen hair density compared to both male morphs (large: $q = 10.98$, $p < 0.0001$; small: $q = 14.82$, $p < 0.0001$).

Females had increased hair density on their abdomens compared to their thoraxes (Kruskal-Wallis, K-W = 38.14, $p < 0.0001$; Dunn's MCT: $Z = 4.67$, $p < 0.0001$). There was no regional variation (e.g., thorax v. abdomen) in hair density within small-morph males, or large-morph males (Dunn's MCT: small: $Z = 0.92$, $p > 0.99$; large: $Z = 0.12$, $p > 0.99$).

Table 2. Differences between male morphs and females in the density of hairs per mm^2 on their dorsal thorax (Kruskal-Wallis with Dunn's MCT) and abdominal surfaces (One-way ANOVA with Tukey's MCT). Letters indicate significant differences ($p < 0.05$) across morphs/sex ($n = 10$) for that region. Asterick indicates significant differences ($p<0.05$) between regions (abdomen vs. thorax) for that morph/sex (Kruskal-Wallis with Dunn's MCT).

Region	Morph/Sex	Mean ± SD	Range
Abdomen - Dorsal			
	LM[a]	617.8 ± 76.82	522.9 – 776.0
	SM[b]	538.2 ± 46.90	479.6 – 626.1
	F[c*]	845.6 ± 69.37	766.0 – 955.8
Thorax - Dorsal			
	LM[a]	604.6 ± 48.86	482.0 – 661.1
	SM[b]	494.4 ± 78.47	411.5 – 656.1
	F[b*]	525.7 ± 44.20	471.2 – 604.0

Figure 3. Differences in hair density of females, large and small morph males, on the dorsal surface. Large morph males have increased thorax hair density compared to small morph males and females (which do not differ in hair density; Kruskal-Wallis: K-W = 11.44, $p = 0.0033$). Females have increased abdominal hair density compared to males, and large-morph males have increased abdominal hair density compared to small-morph males (One-way ANOVA: $F = 59.14$, $df = 27$, $p < 0.0001$). Tukey's or Dunn's MCT: **** = $p < 0.0001$; ** $p < 0.01$; * = $p < 0.05$; ns = not significant

Reflectance of Solar Radiation

Morph/sex significantly impacted mean reflectance on the dorsal abdomen and thorax surfaces (Supplementary Figure 2, Table 3; Two-way RM ANOVA; dorsal-abdomen: $F = 26.32$, $df = 2$, $p < 0.0001$; dorsal-thorax-unshaved: $F = 22.01$, $df = 2$, $p < 0.0001$; dorsal-thorax-shaved: $F = 3.94$, $df = 2$, $p = 0.0314$). Large-morph males had increased mean reflectance across the entire UV-NIR spectrum compared to small-morph males on both the dorsal abdomen and thorax surfaces (Supplementary Figure 2A,B, Supplementary Table 1; Tukey's: all $p > 0.05$).

Table 3. Two-way RM ANOVA with Geisser-Greenhouse Correction of mean reflectance of different morphs (small males, large males, and females) in different wavelength (UV [290-399], VIS [400-700], close NIR [701-1400] and far NIR [1401-2500]) on dorsal surface of the abdomen and thorax (unshaved), the dorsal surface of the thorax (shaved), and the ventral surface of the abdomen.

Comparison region	Source of difference in reflectance	Percent of total difference	F	df	adjusted p value
Abdomen - Dorsal	Wavelength*	77.48	862.3	3	< 0.0001
	Morph	11.19	26.32	2	< 0.0001
	Wavelength x Morph	3.16	17.56	6	< 0.0001
	Individual	5.74	7.10	27	< 0.0001
Abdomen - Ventral	Wavelength*	90.11	711.2	3	< 0.0001
	Morph	0.24	0.65	2	0.53
	Wavelength x Morph	1.12	4.41	6	0.0007
	Individual	5.10	4.48	27	< 0.0001
Thorax - Dorsal (Unshaved)	Wavelength*	88.72	1599	3	< 0.0001
	Morph	6.01	22.01	2	< 0.0001
	Wavelength x Morph	0.09	0.79	6	0.58
	Individual	3.68	7.38	27	< 0.0001
Thorax - Dorsal (Shaved)	Wavelength*	96.13	2045	3	< 0.0001
	Morph	0.48	3.94	2	0.0314
	Wavelength x Morph	0.48	5.12	6	0.0002
	Individual	1.64	3.88	27	< 0.0001

*Geisser-Greenhouse ε for wavelength: Abdomen-Dorsal (0.41), Abdomen-Ventral (0.56), Thorax-Dorsal (Unshaved; 0.53), Thorax-Dorsal (Shaved; 0.59).

The only significant difference between morphs/sexes in the mean reflectance of the shaved dorsal thorax (e.g., cuticle-only) was between small males and females in the UV (Supplementary Figure 2C, Supplementary Table 1; Tukey's: q = 5.70, df = 16.66, p = 0.0301). All differences in mean reflectance between large and small males on the thorax disappeared

326 when the hairs were shaved (Supplementary Table 1; Tukey's: all $p > 0.05$). The presence of
327 thorax hairs significantly increased mean reflectance across the entire UV-NIR spectrum for both
328 small males and large males compared to just the cuticle (Table 4 & Supplementary Table 2;
329 Two-way RM ANOVA with Bonferroni MCT: all $p < 0.05$).

330 **Table 4.** Two-way RM ANOVA with Geisser-Greenhouse Correction of mean reflectance of the
331 thorax, shaved versus unshaved, and abdomen, dorsal versus ventral, at different wavelengths
332 (UV [290-399], VIS [400-700], close NIR [701-1400] and far NIR [1401-2500]) in large males
333 or small males.

Comparison region	Source of difference in reflectance	Percent of total difference	F	df	p value
Large Males					
Thorax	Wavelength*	63.42	688.1	3	< 0.0001
Shaved vs.	Shaved	28.81	198.5	1	< 0.0001
Unshaved	Wavelength x Shaved	3.50	37.97	3	< 0.0001
	Individual	2.61	4.73	18	< 0.0001
Small Males					
Thorax	Wavelength*	90.41	2098	3	< 0.0001
Shaved vs.	Shaved	3.47	26.75	1	< 0.0001
Unshaved	Wavelength x Shaved	3.01	69.85	3	< 0.0001
	Individual	2.33	9.02	18	< 0.0001
Large Males					
Abdomen	Wavelength*	79.35	522.1	3	< 0.0001
Dorsal vs.	Side	8.08	15.52	1	0.0010
Ventral	Wavelength x Side	0.45	2.98	3	0.0393
	Individual	9.37	10.28	18	< 0.0001
Small Males					
Abdomen	Wavelength*	87.33	396.8	3	< 0.0001
Dorsal vs.	Side	0.15	0.39	1	0.54
Ventral	Wavelength x Side	1.56	7.10	3	0.0004
	Individual	6.99	5.29	18	< 0.0001

334
335 *Geisser-Greenhouse ε for wavelength: LM thorax (0.54), SM thorax (0.55), LM abdomen (0.38), SM abdomen
336 (0.39)
337

338 The mean reflectance of the ventral abdominal surface did not differ across morphs/sexes
339 (Supplementary Figure 2D, Table 3; Two-way RM ANOVA: $F = 0.65$, $df = 2$, $p = 0.53$). The
340 ventral surface of the abdomen of large males had reduced mean reflectance across the entire

UV-NIR spectrum compared to the dorsal surface (Table 4 & Supplementary Table 2; Two-way RM ANOVA with Bonferroni: all $p < 0.05$), however the mean reflectance of the dorsal and ventral surface did not differ in small males ($F = 0.39$, $df = 1$, $p = 0.54$).

Absorption of Radiation

The direct beam absorption coefficients of the dorsal thorax and abdominal surfaces of large-morph males were 0.76 ± 0.02 and 0.76 ± 0.06, significantly lower than those of small-morph males, which were 0.83 ± 0.02 and 0.82 ± 0.04 (Figure 4A, Figure 5A, B; One-way ANOVAs, Bonferroni, Thorax: $t = 6.01$, $df = 27$, $p < 0.0001$; Abdomen: $t = 2.61$, $df = 27$, $p = 0.0433$). Females had an abdominal absorption coefficient of 0.75 ± 0.02, statistically similar to large males (One-way ANOVA, Bonferroni: $t = 0.36$, $df = 27$, $p > 0.99$) but lower than small-morph males ($t = 2.97$, $df = 27$, $p = 0.0186$). Females had a thorax absorption coefficient of 0.80 ± 0.03, higher than large males ($t = 3.48$, $df = 27$, $p = 0.0052$) but statistically similar to small males ($t = 2.53$, $df = 27$, $p = 0.0521$).

Figure 4. Difference in direct beam and diffuse absorption coefficients of the dorsal abdomen and thorax between male morphs. A) Difference in absorption of direct beam and diffuse sky solar radiation of the dorsal abdomen, thorax, and shaved thorax cuticular surfaces. Large males and females have reduced absorption coefficients compared to small-morph males on the thorax and abdomen when hairs are present, but when hairs are shaved the absorption coefficients do not vary across male morphs and females. B) There is no difference in the absorption coefficients of male morphs and females when considering reflected solar radiation off a light sand substrate on the ventral surface. **** = $p < 0.0001$; ** $p < 0.01$; * = $p < 0.05$; ns = not significant

Figure 5. Spectral properties of *C. pallida* thorax and abdomen in relation to the irradiance spectrum of direct beam sunlight and sunlight reflected off light sand. Left y-axis represents the percentage of absorbed light at each wavelength, absorbed by the dorsal thorax (A), dorsal abdomen (B), or ventral abdomen (C) cuticle and hairs of *C. pallida* large- and small- males or females (mean, n = 10 each; females in purple, large males in orange, small males in blue). Right axis represents the solar beam irradiance based on solar irradiance distribution standard (Gueymard et al. 2002) in A and B, or the reflected irradiance off light sand (Kokaly et al. 2017) in C (all irradiance in grey).

Females and males did not differ in the direct beam absorption coefficients of their shaved cuticles (Figure 4A; One-way ANOVA, $F = 2.78$, $df = 27$, $p = 0.08$). There was also no difference in the absorption of reflected light by the ventral surfaces of male morphs and females (Figure 4B, Figure 5C; One-way ANOVA, $F = 1.21$, $df = 27$, $p = 0.31$).

Direct beam and diffuse sky radiation was calculated to be 1,178.82 W/m^2 at 1000 h on April 20th. Reflected radiative energy was higher when accounting for wavelength specific effects (329.85 W/m^2) as compared to when applying the same albedo for light sand (0.245) across all wavelengths (288.81 W/m^2); we used 329.85 W/m^2 for all further calculations.

Large-morph males absorbed a mean of 0.36 ± 0.02 W of thermal energy from reflected, direct, and diffuse radiative sources (1.28 ± 0.13 W/g of body mass), compared to 0.26 ± 0.02 W for small-morph males (1.85 ± 0.21 W/g of body mass). If large-morph males had the same reflectance profiles as the averages for small-morph males, they would absorb 0.37 ± 0.03 W of thermal energy (or 1.40 ± 0.15 W/g of body mass, an 8-9% increase in W/g).

Females absorbed a mean 0.28 ± 0.03 W of thermal energy, or 1.40 ± 0.11 W/g of body mass. For all three groups, hairs on the dorsal surface reduced thermal heat flux due to solar radiation; thermal flux for shaved large males was 0.41 ± 0.03 W (1.42 ± 0.17 W/g), for small males was 0.28 ± 0.02 W (1.94 ± 0.23 W/g), and for females was 0.31 ± 0.03 W (1.63 ± 0.12 W/g).

Discussion

Comparative studies of animal solar reflectance (or VIS coloration) often collect data at a macrogeographic scale, and demonstrate the impact of geographic gradients in climate variables (such as ambient temperature or solar radiation) on solar reflectance (e.g., Hegna et al. 2013, Bishop et al. 2016, Munro et al. 2019, Kang et al. 2021, Gomez et al. 2021). However, large differences in ambient temperature can occur within populations when individuals use different microclimates. The 1 cm above-ground microclimate where large male *C. pallida* engaged in their mating behaviors has air temperatures > 8 °C hotter than the 1 m above-ground hovering microclimate used by small males by 1100 am (Barrett et al. 2022), demonstrating that there can be substantial differences in thermal selective pressure across distinct microclimates at the same site. The reduced solar absorption of large-morph males may be a unique thermal adaptation to this very hot microclimate, where they must behave for prolonged periods to successfully access mates (males are known to dig and fight for up to 19 minutes; Alcock et al. 1977).

Morph-specific differences in solar reflectance on the dorsal surface went beyond the VIS, with consistent divergence in reflectance in the NIR. Differences in reflectance between male morphs are likely thermoregulatory adaptations to their distinct, mating microclimates, as extension beyond visible coloration rules out visual selective factors (e.g., anti-predator adaptations) as the sole drivers of reflectance differences. The increased UV-NIR reflectance of

409 large-morph males led to an 8-9% reduction in W/g of absorbed solar energy. Females had
410 intermediate dorsal absorption coefficients: female thorax reflectance profiles were similar to
411 small males, but lower compared to large males, and abdomen reflectance profiles were similar
412 to large males, but increased compared to small males. There was no significant difference in the
413 absorption of reflected irradiance on the ventral surface among morphs and sexes, supporting the
414 hypothesis that differences in reflectance serve to as an adaptation to increase radiative heat gain
415 in cooler microclimates, and decrease it in hotter microclimates.

416 Differences in dorsal reflectance were entirely caused by the hairs; there was no
417 significant difference in the shaved cuticular absorption coefficients of the male morphs or
418 females. Large-morph males had increased hair densities on the thorax and abdominal surfaces
419 compared to small-morph males; however, they had decreased hair density on the abdomen
420 compared to females, despite similar reflectance profiles. This suggests that both hair density, as
421 well as structural features of the hairs (Supplementary Figure 3), may contribute to the
422 reflectance profile differences across male morphs and females. Microstructural features of
423 insect hairs and scales are known to influence their reflective properties in both the NIR and mid-
424 infrared (Shi et al. 2015, Krishna et al. 2020, Krishna et al. 2021).

425 Temperature can vary both spatially and temporally at a given site: across the course of
426 the morning, temperature increased from a low of 16.9 °C to a high of 44.5 °C between 0600 and
427 1100 hrs in the 1 cm microclimate, and from 16.1 °C to 38.9 °C in the 1 m microclimate (Barrett
428 et al. 2022). In male *Colias* butterflies, intraspecific increases in radiative heat gain due to
429 melanization allowed for longer flight periods at cooler air temperatures, increasing access to
430 mating opportunities (Ellers & Boggs 2004, Kingsolver 1983b). The mean body size of the *C.*
431 *pallida* male population increases throughout the morning (both for males foraging, and males

engaged in mating-relevant behaviors; Barrett & Johnson 2022), suggesting smaller males may use their darker coloration to increase radiative heat gain and increase their access to mates during cooler early morning periods when large males are not yet as prevalent in the population.

An additional implication of this work relates to unraveling the various factors that may lead to stabilizing selection for dimorphic body morphologies in ART systems. Generally, it has been hypothesized that bird predation may select against the large-morph male mating advantage in the *C. pallida* system, producing persistent size variation and two distinct morphs (Alcock 1995). However, bird predation is variable across field sites (Alcock 1995) while size dimorphism is not; in addition, large-morph males are not behaviorally wary of predation events (which might be expected if predation was as a significant selective force; Alcock 2013, Barrett pers. obs.). An alternate hypothesis, better supported by our data, relates the continued existence of two microclimate-specialized morphs to the thermoregulatory selective pressures of the available microclimates. Males of an intermediate size and UV-NIR reflectance profile would be disadvantaged due to higher metabolic rates (and higher metabolic heat production) when using small male mating strategies (in other bees with intraspecific body size variation, smaller individuals have increased power efficiency in flight without any additional metabolic cost (Grula et al. 2021)), while also disadvantaged due to their increased solar absorptivity when using the large male mating strategies. Individual morphological specialization in relation to body form and reflectance may potentially facilitate the stability of the male *C. pallida* ART system.

Our study demonstrates the importance of shortwave reflectance as an intraspecifically variable thermoregulatory adaptation. Variation in reflectance of shortwave radiation, and other morphological adaptation to thermal pressures (such as larger body sizes), may alter the

necessity for physiological thermoregulatory differences – for example, large morph males that can avoid overheating in the sun due to their reduced relative solar heat load may not need increased thermal tolerances to survive (see Barrett et al. 2022). The interplay between these morphological and physiological thermoregulatory strategies thus deserves greater attention. In addition, this variation suggests individuals within populations may find their fitness-relevant behaviors to be differently constrained by increasing global temperatures due to the effects of variation in shortwave radiative heat gain on their energy budget. If thermoregulatory selective pressures play a role in maintaining size or behavioral variation within species (such as ART systems), this suggests that climate change may have impacts that stretch beyond species-level diversity – impacting intraspecific morphological and behavioral diversity as well.

We demonstrate that individual differences, often overlooked, may be important for understanding the selective pressures acting on individuals to generate evolutionary adaptations to fine-scale ecological variation. Future studies should thus pay greater attention to the effects of morphological, physiological, or behavioral variation between conspecifics, which may have important consequences for understanding proximate and ultimate causes of ecological reflectance and coloration patterns.

Acknowledgements: This work would not have been possible without the support of Kathryn Busby, Logan Schoolcraft, and Stephen Buchmann. Offir Cohen assisted with making the aperture, and spectrophotometer training. Funding for travel and supplies came from an American Philosophical Society Lewis and Clark Grant; an Entomological Society of America Student Research Travel Award to MB for work carried out in the Frederick Seitz Materials Research Laboratory Central Research Facilities, University of Illinois; a Microscopy Training Fellowship Award from the American Microscopical Society funded the work conducted at

Drexel University's Core Research Facilities. MB was not a National Science Foundation postdoctoral fellow while completing this work but is an NSF postdoctoral fellow at the time of publication: any opinions, findings, conclusions, or recommendations expressed in this manuscript are the authors, and do not necessarily reflect the views of the NSF.

References

Alcock J (1976) The social organization of male populations of *Centris pallida* (Hymenoptera, Anthophoridae). Psyche 83:121-131.

Alcock J (1995) Persistent size variation in the anthophorine bee *Centris pallida* (Apidae) despite a large male mating advantage. Ecol Entomol 20:1-4.

Alcock J (2013) Role of body size in the competition for mates by males of *Centris pallida* (Anthophorinae: Hymenoptera). Southwest Nat 58:427-430.

Alcock J, Jones E, Buchmann S (1976) Location before emergence of the female bee, *Centris pallida*, by its male (Hymenoptera: Anthrophoridae). J Zool 179:189-199.

Alcock J, Jones E, Buchmann S (1977) Male mating strategies in the bee *Centris pallida* Fox (Anthophoridae: Hymenoptera). Am Nat 111:145-155.

Amore V, Hernández MIM, Carrascal LM, Lobo JM (2017) Exoskeleton may influence the internal body temperatures of Neotropical dung beetles (Col. Scarabaeinae). PeerJ 5: e3349.

Barrett M, Tigreros N, Davidowitz G, O'Donnell S (2022) Adaptive variation in sex and male size morph critical thermal maxima in *Centris pallida* desert bees. SSRN preprint, DOI: 10.2139/ssrn.4085466

Barrett M, Johnson MG (2022) Don't get a big head: Centris pallida (Hymenoptera: Apidae) male head widths decrease across five decades. BioRxiv preprint, DOI:

https://doi.org/10.1101/2022.05.27.493633

Baudier KM, D'Amelio CL, Malhotra R, O'Connor MP, O'Donnell S (2018) Extreme climatic variation shapes the evolution of thermal tolerance at multiple scales. Am Nat 192:347-359.

Baudier KM, Mudd AE, Erickson SC, O'Donnell S (2015) Microhabitat and body size effects on heat tolerance: Implications for responses to climate change (army ants: Formicidae, Ecitoninae). J Anim Ecol 84: 1322 – 1330.

Bishop TR, Robertson MP, Gibb H, van Rensburg BJ, Braschler B, Chown SL … Parr CL (2016) Ant assemblages have darker and larger members in cold environments. Global Ecol Biogeo 25:1489-1499.

Bogert CM (1949) Thermoregulation in reptiles, a factor in evolution. Evol 3: 195–211.

Cerdá X, Retana J, Cros S (1998) Critical thermal limits in Mediterranean ant species: trade-off between mortality risk and foraging performance. Functional Ecol 12:45–55.

Chappell M (1984) Temperature regulation and energetics of the solitary bee *Centris pallida* during foraging and intermale mate competition. Physiol Zool 57:215-225.

Clusella-Trullas S, van Wyk JH, Spotila JR (2007) Thermal melanism in ectotherms. J Therm Biol 32:235-245.

Cole LC (1943) Experiments on toleration of high temperature in lizards with reference to adaptive coloration. Ecol 24:94-108.

Cuesta E, Lobo JM (2019) Visible and near-infrared radiation may be transmitted or absorbed differently by beetle elytra according to habitat preference. PeerJ 7: e8104.

Ellers J, Boggs CL (2004) Functional ecological implications of intraspecific differences in wing melanization in *Colias* butterflies. Biol J Linn Soc 82: 79-87.

524 Gomez D, Pinna C, Pairraire J, Arias M, Barbut J, Pomerantz A, Daney de Marcillac W, Berthier
525 S, Patel N, Andraud C, Elias M (2021) Wing transparency in butterflies and moths:
526 Structural diversity, optical properties, and ecological relevance. Ecol Monographs 91:
527 e01475.
528 GraphPad Software. 2021. GraphPad Prism v 9.1.2 for Windows. La Jolla, CA.
529 Grula CC, Rinehart JP, Greenlee KJ, Bowsher JH (2021) Body size allometry impacts flight-
530 related morphology and metabolic rates in the solitary bee, *Megachile rotundata.* J Insect
531 Physiol 133: 104275.
532 Gueymard CA, Myers D, Emery K (2002) Proposed reference irradiance spectra for solar energy
533 systems testing. Solar Energy 73:443-467.
534 Hegna RH, Nokelainen O, Hegna JR, Mappes J (2013) To quiver or to shiver: Increased
535 melanization benefits thermoregulation, but reduces warning signal efficacy in the
536 wood tiger moth. Proc R Soc B 280: 20122812.
537 Huey RB, Kingsolver JG (1989) Evolution of thermal sensitivity of ectotherm performance.
538 Trends Ecol Evol 4:131-135.
539 Kang C, Im S, Lee WY, Choi Y, Stuart-Fox D, Huerta B (2021) Climate predicts both visible
540 and near-infrared reflectance in butterflies. Ecol Lett 24: 1869-1879.
541 Kaspari M, Clay NA, Lucas J, Yanoviak SP, Kay A (2014) Thermal adaptation generates a
542 diversity of thermal limits in a rainforest ant community. Glob Change Biol: doi:
543 10.1111/gcb.12750.
544 Kingsolver JG (1983a) Ecological significance of flight activity in *Colias* butterflies:
545 implications for reproductive strategy and population structure. Ecology 64: 546-551.
546 Kingsolver JG (1983b) Thermoregulation and flight in *Colias* butterflies: elevational patterns

547 and mechanistic limitations. Ecology 64: 534-545.
548 Kokaly RF, Clark RN, Swayze GA, Livo KE, Hoefen TM, Pearson NC, Wise RA, Benzel WM,
549 Lowers HA, Driscoll RL, Klein AJ (2017) USGS Spectral Library Version 7: U.S.
550 Geological Survey Data Series 1035. 61 p. https://doi.org/10.3133/ds1035.
551 Krishna A, Nie X, Briscoe AD, Jee J (2021) Air temperatures drive the evolution of mid-infrared
552 optical properties of butterfly wings. Scientific Reports 11: 24143.
553 Krishna A, Nie X, Warren AD, Llorente-Bousquets JE, Briscoe AD, Lee J (2020) Infrared
554 optical and thermal properties of microstructures in butterfly wings. PNAS 117: 1566-
555 1572.
556 Marion B (2020) Albedo data sets for bifacial PV systems: Preprint. Golden, CO: National
557 Renewable Energy Laboratory. NREL/CP-5K00-75924.
558 https://www.nrel.gov/docs/fy21osti/75924.pdf.
559 Medina I, Newton E, Kearney MR, Mulder RA, Porter WP, Stuart-Fox D (2018) Reflection of
560 near-infrared light confers thermal protection in birds. Nat Comm 9: 3610.
561 Munro JT, Medina I, Walker K, Moussalli A, Kearkey MR, Dyer AG, Garcia J, Rankin KJ,
562 Stuart-Fox D (2019) Climate is a strong predictor of near-infrared reflectance but a poor
563 predictor of colour in butterflies. Proc Royal Soc B 286:20190234.
564 Peterson WA, Dirmhirn I (1981) The ratio of diffuse to direct solar irradiance (perpendicular to
565 the sun's rays) with clear skies – a conserved quantity through the day. J Applied
566 Meteorol 20:826-828.
567 Schofield SF, Bishop TR, Parr CL (2016) Morphological characteristics of ant assemblages
568 (Hymenoptera: Formicidae) differ among contrasting biomes. Myrmecological News
569 23:129-137.

570 Schultz TD, Hadley NF (1987) Structural colors of tiger beetles and their role in heat transfer
571 through the integument. Physiol Zool 60:737-745.
572 Shi NN, Tsai C, Camino F, Bernard GD, Yu N, Wehner R (2015) Keeping cool: Enhanced
573 optical reflection and radiative heat dissipation in Saharan silver ants. Science 349:298-
574 301.
575 Smith KR, Cadena V, Endler JA, Porter WP, Kearney MR, Stuart-Fox D (2016) Colour change
576 on different body regions provides thermal and signaling advantages in bearded dragon
577 lizards. Proc R Soc Lond B 283:20160626.
578 Snelling RR (1984) Studies on the taxonomy and distribution of American Centridine bees
579 (Hymenoptera: Anthophoridae). Contributions in Science 347:1-69.
580 Spacht DE, Gantz JD, Devlin JJ, McCabe EA, Lee Jr. RE, Denlinger DL, Teets NM (2021) Fine-
581 scale variation in microhabitat conditions influences physiology and metabolism in an
582 Antarctic insect. Oecologia 197: 373-385.
583 Spicer J, Gaston K (1999) *Physiological diversity: Ecological implications.* Blackwell Science,
584 Oxford, UK.
585 Stuart-Fox D, Newton E, Clusella-Trullas S (2017) Thermal consequences of colour and near-
586 infrared reflectance. Phil Trans R Soc B 372:20160345.
587 Stupski SD, Schilder RJ (2021) Operative temperature analysis of the honey bee *Apis mellifera.* J
588 Exp Biol 224:jeb231134.
589 van Dyck H, Matthysen E (1998) Thermoregulatory differences between phenotypes in the
590 speckled wood butterfly: Hot perchers and cold patrollers? Oecologia 114:326-334.
591 Wang L, Franklin AM, Black JR, Stuart-Fox D (2021) Heating rates are more strongly
592 influenced by near-infrared than visible reflectance in beetles. J Exp Biol 224: jeb242898.

Willig MR, Kaufman DM, Stevens RD (2003) Latitudinal gradients of biodiversity: pattern, process, scale, and synthesis. Ann Rev Ecol Evol Systematics 34:273-309.

Supplementary Materials

Supplementary Figure 1. Difference in coloration of *C. pallida* hairs on the thoraxes and abdomens of large- and small-morph males and females. All photos taken at 85X magnification on a DinoLite AM4915ZT.

Supplementary Figure 2. Reflectance of females, large males, and small males on the dorsal and ventral abdominal surface and dorsal thorax surface when shaved or unshaved. A) Differences in reflectance between large males, small males, and females on the dorsal surface of the thorax (Two-way RM ANOVA: $F = 22.01$, $df = 2$, $p < 0.0001$; MCT: Supplementary Table 1) and B) of the abdomen ($F = 26.32$, $df = 2$, $p < 0.0001$). C) The only significant difference in reflectance on the shaved dorsal thorax (e.g., cuticle-only) was between small males and females in the UV ($F = 3.94$, $df = 2$, $p = 0.0314$; MCT: UV SM-Female, $q = 5.70$, $df = 16.66$, $p = 0.0301$; all other comparisons, $p > 0.05$). D) There was no difference in mean reflectance between male morphs and females on the ventral surface of the abdomen ($F = 0.65$, $df = 2$, $p = 0.53$). Thick, solid or dashed lines represent mean reflectance; dotted lines are SD. The dotted, vertical line at 700 nm separates the VIS and NIR wavelengths.

Supplementary Figure 3. Large male thorax hair characteristics. Left) The hairs of large-morph males have a round cross-section, and are covered in striations (5000X). **Right)** Close-up of striations on the exterior surface of large-morph male thorax hairs (8500X). The somewhat regular striations are reminiscent of the structure of the highly reflective hairs of the Saharan silver ant (in Shi et al. 2015).

Supplementary Table 1. Tukey's multiple comparisons test (following two-way RM ANOVA with Geisser-Greenhouse Correction) of mean reflectance of small males (SM), large males (LM), and females (F) in the UV (290-399), VIS (400-700), close NIR (701-1400) and far NIR (1401-2500) on dorsal surface of the abdomen and thorax (unshaved and shaved).

Comparison Region	Wave-lengths	Comparison Groups	q	df	adjusted p value
Abdomen - Dorsal	*UV*				
		LM vs. SM	6.60	11.47	**0.0182**
		LM vs. F	4.35	11.14	0.20
		SM vs. F	4.77	17.90	0.10
	VIS				
		LM vs. SM	6.99	13.48	**0.0084**
		LM vs. F	1.50	11.34	> 0.99
		SM vs. F	9.92	16.17	**0.0001**
	close NIR				
		LM vs. SM	8.29	16.84	**0.0008**
		LM vs. F	0.20	12.88	> 0.99
		SM vs. F	11.35	15.07	**< 0.0001**
	far NIR				
		LM vs. SM	7.58	17.53	**0.0020**
		LM vs. F	0.69	13.73	> 0.99
		SM vs. F	9.15	15.16	**0.0004**
Thorax w/Hair	*UV*				
		LM vs. SM	11.32	14	**< 0.0001**
		LM vs. F	7.78	12.69	**0.0039**
		SM vs. F	6.05	17.49	**0.0174**
	VIS				
		LM vs. SM	10.69	17.74	**< 0.0001**
		LM vs. F	6.03	17.93	**0.0173**
		SM vs. F	3.96	17.42	0.26
	close NIR				
		LM vs. SM	6.67	17.97	**0.0069**
		LM vs. F	3.37	17.41	0.46
		SM vs. F	2.74	17.64	0.73
	far NIR				
		LM vs. SM	6.04	17.97	**0.0170**
		LM vs. F	3.11	17.77	0.57
		SM vs. F	2.50	17.58	0.81
Thorax Shaved	*UV*				
		LM vs. SM	0.24	12.5	> 0.99
		LM vs. F	2.78	11.01	0.71
		SM vs. F	5.70	16.66	**0.0301**
	VIS				
		LM vs. SM	0.05	15.30	> 0.99
		LM vs. F	3.42	17.98	0.44

	SM vs. F	3.99	14.99	0.26
close NIR				
	LM vs. SM	3.14	12.85	0.56
	LM vs. F	1.70	15.17	0.98
	SM vs. F	1.87	16.72	0.96
far NIR				
	LM vs. SM	4.44	13.00	0.17
	LM vs. F	2.96	17.05	0.63
	SM vs. F	1.26	14.97	> 0.99

Supplementary Table 2. Bonferroni's multiple comparisons test (following two-way RM ANOVA with Geisser-Greenhouse Correction) of mean reflectance of the thorax, shaved versus unshaved, and abdomen, dorsal versus ventral, at different wavelengths (UV [290-399], VIS [400-700], close NIR [701-1400] and far NIR [1401-2500]) in large males or small males.

Morph	**Comparison**	**Wave length**	**t**	**df**	**adjusted p value**
Large Males - Thorax	Shaved vs. Unshaved				
		UV	5.46	13.22	0.0004
		VIS	17.59	9.76	< 0.0001
		cNIR	12.52	16.97	< 0.0001
		fNIR	10.30	17.77	< 0.0001
Small Males - Thorax	Shaved vs. Unshaved				
		UV	4.95	11.91	0.0014
		VIS	8.77	9.40	< 0.0001
		cNIR	6.43	11.21	0.0002
		fNIR	4.53	12.50	0.0025
Large Males - Abdomen	Dorsal vs. Ventral				
		UV	5.61	14.06	0.0003
		VIS	5.31	15.66	0.0003
		cNIR	2.82	17.93	0.0458
		fNIR	3.19	17.99	0.0205

Figure 1

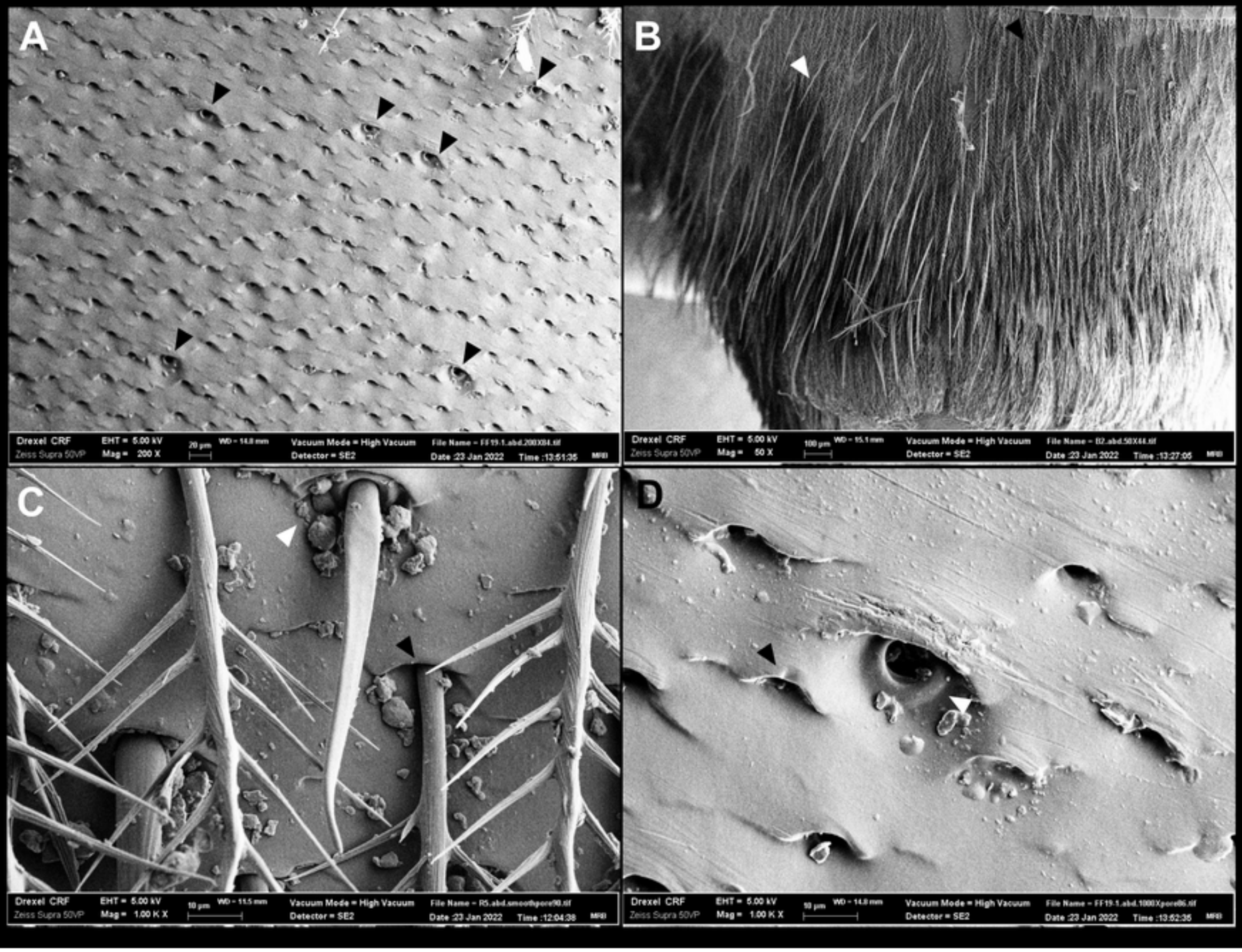
A
Drexel CRF
Zeiss Supra 50VP
EHT = 5.00 kV
Mag = 200 X
20 µm
WD = 14.8 mm
Vacuum Mode = High Vacuum
Detector = SE2
Date :23 Jan 2022
Time :13:51:35
B
Drexel CRF
Zeiss Supra 50VP
EHT = 5.00 kV
Mag = 50 X
100 µm
WD = 15.1 mm
Vacuum Mode = High Vacuum
Detector = SE2
Date :23 Jan 2022
Time :13:27:05
C
Drexel CRF
Zeiss Supra 50VP
EHT = 5.00 kV
Mag = 1.00 K X
10 µm
WD = 15.5 mm
Vacuum Mode = High Vacuum
Detector = SE2
Date :23 Jan 2022
Time :12:04:38
D
Drexel CRF
Zeiss Supra 50VP
EHT = 5.00 kV
Mag = 1.00 K X
50 µm
WD = 14.0 mm
Vacuum Mode = High Vacuum
Detector = SE2
Date :23 Jan 2022
Time :13:52:35

Figure 2

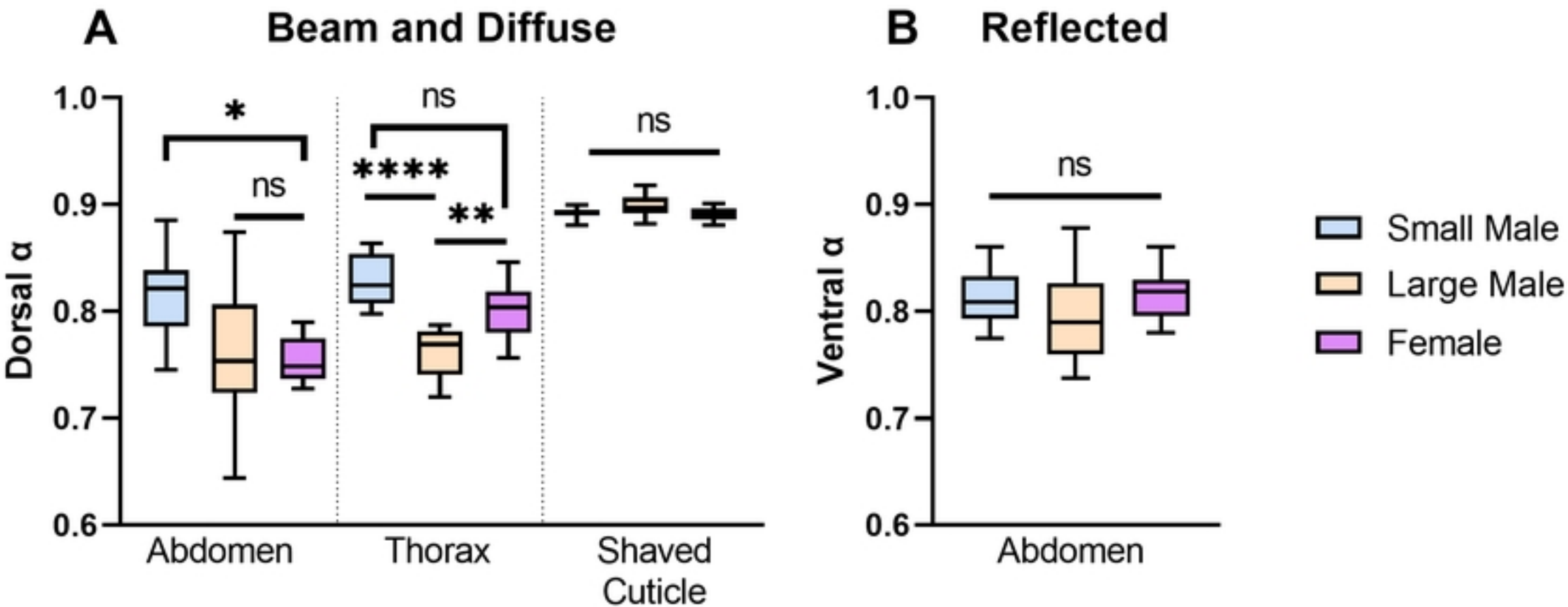
A
Beam and Diffuse
B
Reflected
Dorsal α
Ventral α
1.0
0.9
0.8
0.7
0.6
*
ns
****
**
ns
ns
Abdomen
Thorax
Shaved Cuticle
Abdomen
Small Male
Large Male
Female

Figure 4

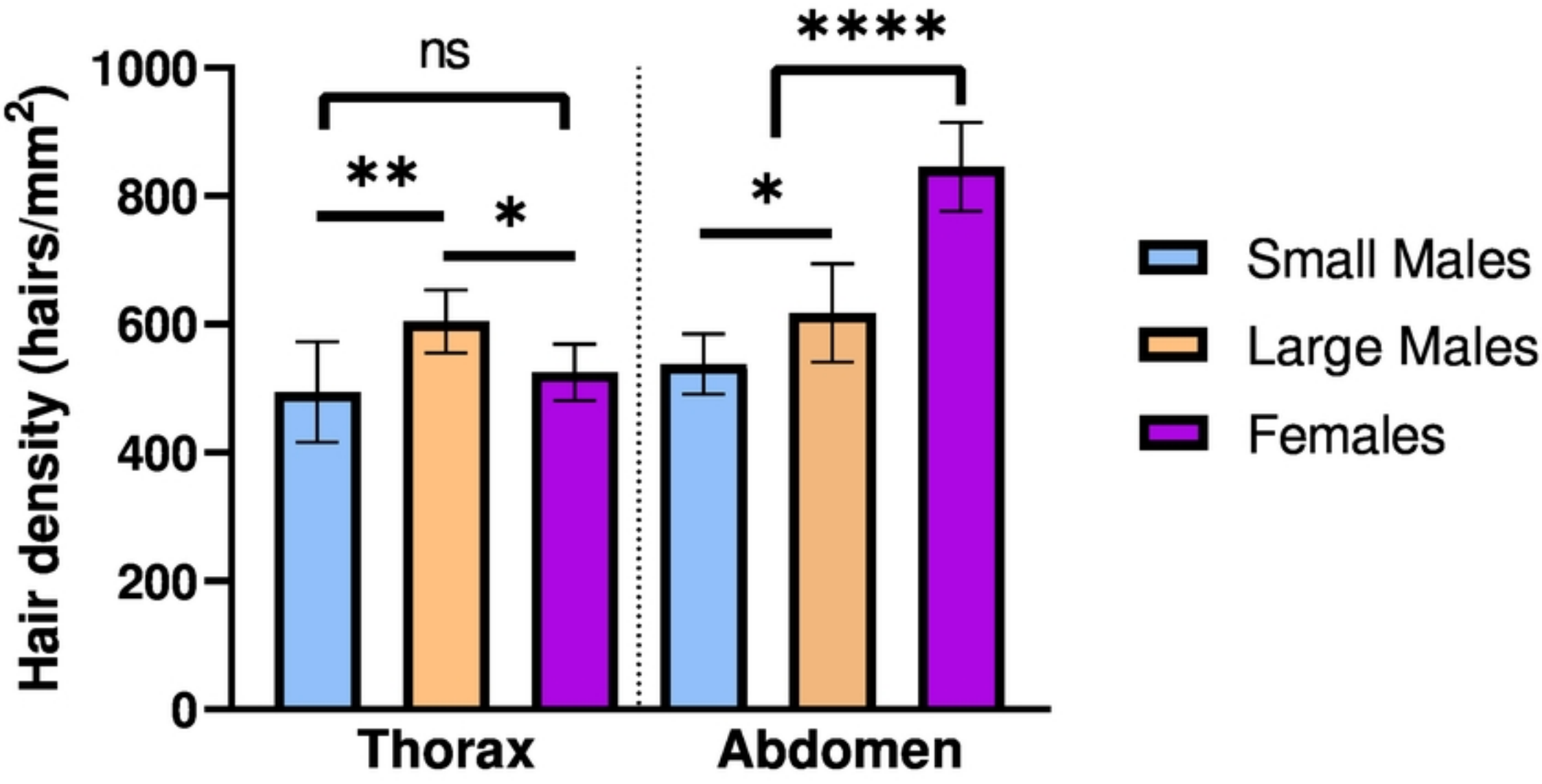
Hair density (hairs/mm^2)
1000
800
600
400
200
0
ns
**
*
****
*
Thorax
Abdomen
Small Males
Large Males
Females

Figure 3

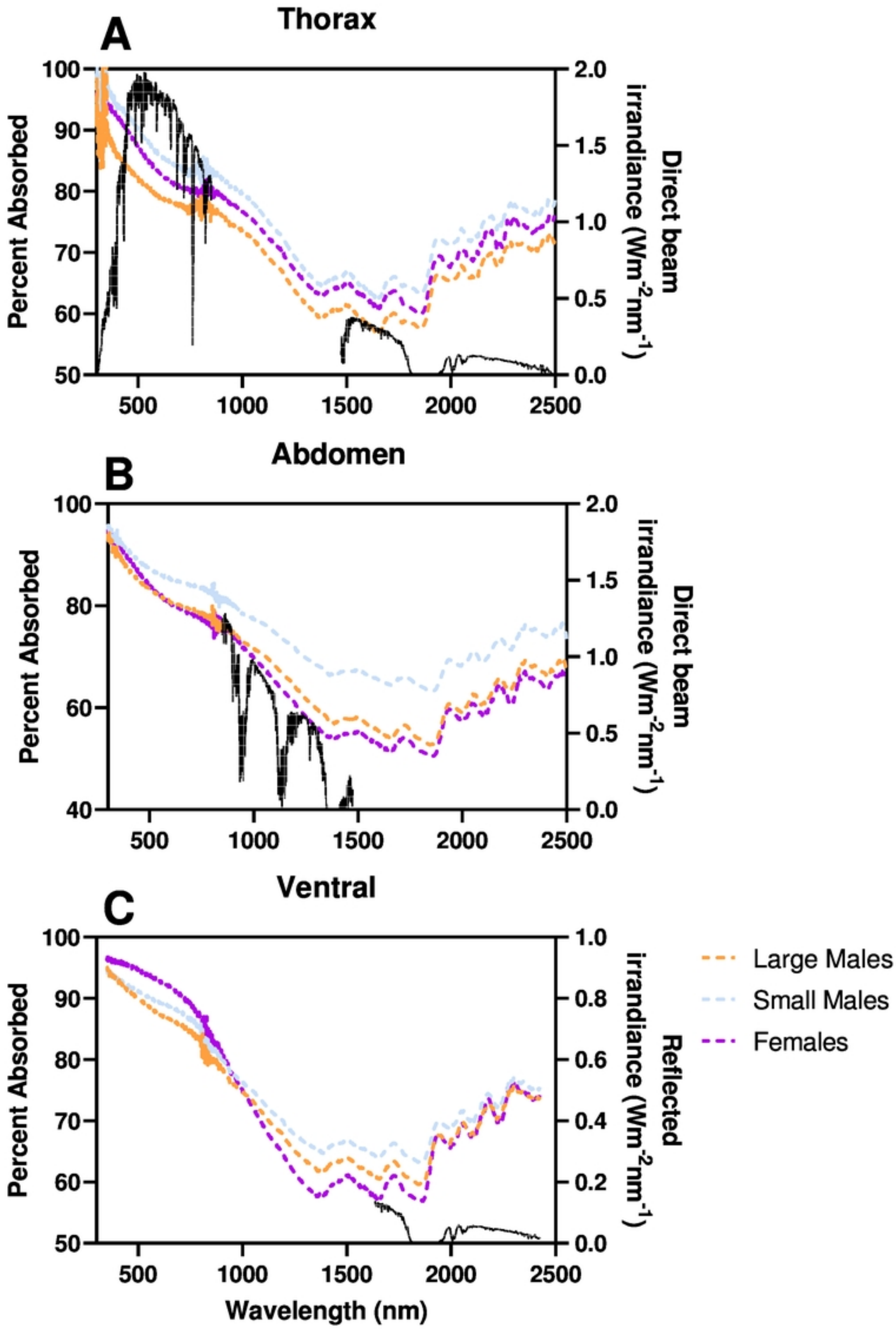
A
Thorax
Percent Absorbed
Direct beam irrandiance (Wm-2nm-1)
B
Abdomen
Ventral
C
Reflected irrandiance (Wm-2nm-1)
Wavelength (nm)
Large Males
Small Males
Females

Figure 5